Sustainable Energy & Fuels

ROYAL SOCIETY OF CHEMISTRY

PAPER

View Article Online
View Journal | View Issue

Cite this: *Sustainable Energy Fuels*, 2021, **5**, 2055

In situ synthesis of methane using Ag–GDC composite electrodes in a tubular solid oxide electrolytic cell: new insight into the role of oxide ion removal†

Saheli Biswas,[b] Aniruddha P. Kulkarni, *[a] Daniel Fini,[a] Sarbjit Giddey[a] and Sankar Bhattacharya [b]

The conversion of waste CO_2 into energy carrier fuels ("electrofuels") using renewable energy (RE) in solid oxide electrolytic cells (SOECs) is a fast-emerging technology. Methane is one such potential electrofuel under consideration for the transport and local storage of RE. Most of the synthetic methane generation routes under investigation are two-step processes utilizing SOECs as a source of either H_2 or syngas (H_2/CO mixture) that undergoes methanation in a subsequent thermochemical reactor. However, the technology for direct one-step *in situ* synthesis of methane in SOECs is still at an early stage. This work demonstrates, for the very first time, purely electrolytic one-step methane generation in a symmetric, tubular SOEC in the temperature range of 500–700 °C in the absence of any methanation catalyst simply by electrolysing a mixture of H_2 and CO_2. The non-attainment of methane at OCV and in contrast methane generation under applied potential indicate that the phenomenon is completely driven by electrochemical processes. Interestingly, at all temperatures, the first trace of methane was detected at a certain minimum value of current density, and that value of current density increased non-linearly with temperature. The extent of methane generation appears to be effectively shifted by increasing the rate of oxide ion removal from the cell. Thus, we hypothesize that the electrochemical oxygen pumping phenomenon is a facilitator of such a direct methane synthesis reaction envisaged during *in situ* methanation in SOECs.

Received 23rd December 2020
Accepted 18th February 2021

DOI: 10.1039/d0se01887b

rsc.li/sustainable-energy

1. Introduction

The gradual depletion of fossil fuels, along with the catastrophic levels of greenhouse gas emissions, has made a compelling case for the exploration and deployment of renewable energy-powered electrochemical pathways of fuel synthesis. One such route is known as Power-to-X, where X can be either hydrogen or a hydrogen carrier, such as ammonia, methane or methanol. The electrolytic synthesis of methane in solid oxide electrolytic cells (SOECs) is of great interest for various reasons. For example, an energy efficiency (defined by the energy content of methane produced to the energy input) of ~95% is theoretically well predicted at the cell level.[1] This is primarily due to lower overpotential losses when using SOECs. In addition, SOECs can be used for *in situ* methane synthesis by electrolysing CO_2 in the presence of H_2 (from renewable sources) with the right combination of the electrocatalyst and process conditions.

However, this route of methane synthesis is an early stage technology, with very limited studies on the fundamental mechanism or development of materials tailored for the methanation process. Xie *et al.*[2] were one of the first to perform *in situ* methanation using a composite of lanthanum-doped strontium titanate ($La_{0.2}Sr_{0.8}TiO_{3+\delta}$, or LST) and gadolinia-doped ceria ($Gd_{0.2}Ce_{0.8}O_{1.95}$, or GDC) as a cathode with 8 mol% yttria (Y_2O_3)-stabilised zirconia (ZrO_2) (YSZ) as the electrolyte, and a lanthanum strontium manganite ($La_{0.8}Sr_{0.2}$-$MnO_{3-\delta}$, or LSM) and YSZ composite anode. They also used an additional layer of an iron catalyst placed in direct contact with the cathode. At 650 °C, about 2.8% methane was generated at atmospheric pressure. Bierschenk *et al.*[3] obtained 2% methane from H_2/CO_2 (4 : 1) electrolysis in a single-zone SOEC comprising an Ni–YSZ cathode, YSZ electrolyte and LSM–YSZ anode, where the entire cell was operated at 600 °C under a current of 0.4 A. Li *et al.*[4] reported a methane yield of 0.02% at 2 V and 650 °C by co-electrolysing H_2O/CO_2 (2 : 1) using an Ni–YSZ cathode, scandia (Sc_2O_3)-stabilised zirconia (ScSZ) electrolyte and LSM–ScSZ anode. Recently, Luo *et al.*[12] studied the

[a]*CSIRO Energy, Private Bag 10, Clayton South 3169, Victoria, Australia. E-mail: Aniruddha.Kulkarni@csiro.au*

[b]*Department of Chemical Engineering, Monash University, VIC 3800, Australia*

† Electronic supplementary information (ESI) available. See DOI: 10.1039/d0se01887b

effect of pressure on steam/CO_2 co-electrolysis in a single-zone SOEC comprising an Ni–ScSZ cathode, ScSZ electrolyte and LSM–ScSZ anode at 650 °C. They concluded that increasing the pressure from 1 bar to 4 bars increased the methane yield from 2.8% to 28.7%. However, all three groups used a Ni-cermet cathode, which has significant catalytic activity towards methanation. Some researchers have shown evidence of *in situ* methane synthesis in a dual-temperature-zone SOEC, where the first zone (SOEC) is kept at a high temperature (650–800 °C) that gradually drops to ~250 °C in the subsequent Fischer–Tropsch (F–T) zone. The rationale here is that CO_2 electrolysis, being an endothermic reaction, is favoured at higher temperatures, whereas methanation is highly exothermic and therefore favourable at lower temperatures (250–350 °C). Thus, the SOEC zone being operated between 650 and 800 °C generates sufficient CO, both from CO_2 electrolysis and the reverse water gas shift reaction (RWGS), to undergo methanation in the low-temperature F–T zone in the presence of H_2. The H_2 can either be produced *in situ* from steam electrolysis or fed directly to the fuel electrode as a H_2/CO_2 mixture. In one such design, Chen *et al.*[5] conducted *in situ* methanation using a Ni-cermet cathode, YSZ electrolyte and LSM–YSZ anode. The SOEC zone was operated at 800 °C at an applied potential of 1.3 V, and the temperature was gradually decreased to 250 °C in the F–T regime. They obtained a maximum methane yield of 11.8%. In another study, Chen *et al.*[6] showed that increasing the cell pressure to 3 bar while maintaining the SOEC part at 800 °C and the F–T zone at 250 °C increased the methane yield to 17%. Further increases in pressure had no significant effect on the methane yield, due to the synergistic effect of pressure on the methanation reaction rate and current density. Note that all such experiments have been conducted with Ni or Fe-based methanation catalysts, either present within the cathode (Ni-cermet) or kept as a separate layer in the F–T zone.[5,6] Thus, to the best of our knowledge, no trace of *in situ* methane has yet been reported, where H_2/CO_2 electrolysis or steam/CO_2 co-electrolysis has been carried out in a single-zone, high-temperature SOEC without a subsequent F–T zone and in the absence of any methanation catalyst. Such an investigation is essential to better comprehend the rate-determining step/s of *in situ* methanation in a single-zone, high or intermediate-temperature SOEC.

In this work, we aimed to evaluate a composite of Ag and 10 mol% GDC ($Gd_{0.1}Ce_{0.9}O_{2-\delta}$) as a potential electrode for *in situ* methane synthesis using a H_2/CO_2 mixture and to qualitatively determine the role of thermodynamic equilibrium in this process. A porous composite of Ag and $Gd_{0.2}Ce_{0.8}O_{2-\delta}$ previously demonstrated superior performance in CO_2 electroreduction[7] at 800 °C, but has not been tested for *in situ* methanation using an H_2/CO_2 (4 : 1) mixture. GDC has the following advantages: (1) it shows mixed ionic electronic conductivity under a reducing atmosphere;[8] (2) it possesses sufficient ionic conductivity between 500 and 700 °C; (3) as ceria is highly reducible, it increases CO_2 adsorption as evidenced by heterogeneous catalysis.[9,10] We added Ag because it improves the uniformity of the cathode microstructure,[7,11] which reduces polarisation losses and improves cell performance. Ag also improves adhesion between GDC and the most common electrolyte, 8 mol% YSZ,[7,11] which implies an increment in the effective triple phase boundary (TPB) area that is likely to improve CO_2 electroreduction.

Most importantly, we avoided the use of any methanation catalyst in this work to ensure a better understanding of the electrocatalytic activity of Ag–GDC towards *in situ* methanation. With the electrode chosen in this work, *in situ* methanation from H_2/CO_2 electrolysis is expected to follow a complex pathway consisting primarily of four different steps occurring at the cathode, as mentioned elsewhere.[12] They include CO_2 hydrogenation to methane *via* methanation (eqn (1)) and to CO *via* RWGS (eqn (2)); CO_2 electroreduction to CO (eqn (3)); and CO hydrogenation to methane (eqn (4)). The anodic reaction involves oxygen evolution (eqn (5)).

At the cathode:

$$CO_2 + 4H_2 = CH_4 + 2H_2O \ (\Delta H_{1023K} = -164 \text{ kJ mol}^{-1}) \quad (1)$$

$$CO_2 + H_2 = CO + H_2O \ (\Delta H_{1023K} = 41.2 \text{ kJ mol}^{-1}) \quad (2)$$

$$CO_2 + 2e^- = CO + O^{2-} \ (\Delta H_{1023K} = 282 \text{ kJ mol}^{-1}) \quad (3)$$

$$CO + 3H_2 = CH_4 + H_2O \ (\Delta H_{1023K} = -206.1 \text{ kJ mol}^{-1}) \quad (4)$$

At the anode:

$$O^{2-} = \tfrac{1}{2}O + 2e^- \quad (5)$$

Appreciable methane generation can be ascertained only when the cathode exhibits sufficient catalytic activity for eqn (1)–(4) to occur. This is especially the case for CO_2 electroreduction, the kinetics of which are very sluggish.[13–15] Moreover, the accurate control of the ratio of H_2 to CO in steam/CO_2 co-electrolysis is quite difficult as opposed to H_2/CO_2 electrolysis, especially considering the large area of our cell (33 cm^2). Thus, we restricted our initial experiments to the electrolysis of dry CO_2 only, followed by a mixture of H_2/CO_2 using electrolyte-supported, symmetric tubular cells. We used the state-of-the-art electrolyte YSZ with an Ag–GDC composite electrode for both dry CO_2 and H_2/CO_2 electrolysis at 500–700 °C, as detailed in Section 2.

2. Results and discussion

2.1 Electrochemical performance of the Ag–GDC composite electrode for dry CO_2 electrolysis

Fig. 1A shows the current–voltage (*V–I*) curves (corrected for lead wire resistances) for an A-GDC/YSZ symmetric tube cell tested at 500, 600, 700 and 800 °C with dry CO_2; Fig. S1B in the ESI† shows the corresponding impedance spectra under open-circuit conditions.

As expected, the current increased as the temperature rose, with a maximum current density of about 140 mA cm^{-2} obtained at an applied potential of 1.5 V at 800 °C. The increase in current density can be attributed to the synergistic effect of decreased electrolyte ohmic resistance (R_{ohm}) and reduced electrode polarisation resistance (R_{pol}) due to improved

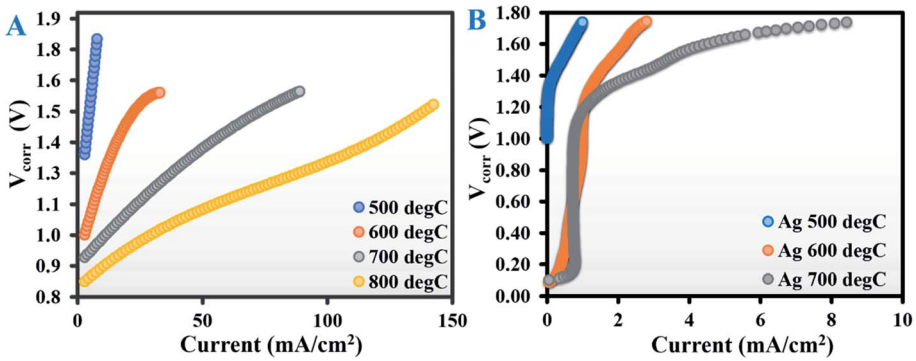

Fig. 1 Current–voltage curves (corrected for lead wire resistance) of a tubular solid oxide electrolysis cell, recorded during electrochemical reduction of dry CO_2 at (A) 500, 600, 700 and 800 °C with the Ag–GDC composite electrode, and (B) 500, 600 and 700 °C with the bare Ag electrode.

kinetics. The electrochemical impedance spectroscopy (EIS) spectra at all test temperatures (Fig. S1B in the ESI†) were composed of two distinct arcs, which can be nominally separated into high frequency (HF, ranging from 1000 to 5 Hz) and low frequency (LF, ranging from 5 to 0.1 Hz). Based on previous reports,[8,13,14,16–19] the LF arc can be ascribed to slower processes related to diffusion-limited mass transfer, dissociative adsorption of CO_2, and desorption of CO or the even surface-exchange reaction of CO/CO_2 at the gas–cathode interface. The HF arc is usually related to the less energy-intensive oxygen evolution reaction (eqn (5)) occurring at the anode.

The analysis of R_{ohm} values (calculated from the intercepts of the HF arcs on the real axis) in conjunction with the *V–I* curves showed that beyond 1.4 V, the increase in current as a function of temperature was roughly proportional to the decrease in R_{ohm}. This indicates that in the high-temperature regime, there was a dominating contribution from ohmic losses above 1.4 V, whereas below 1.4 V the process might be controlled by polarisation. The mechanism of the reaction in SOECs is a complex phenomenon and is not yet well understood for operation in electrolytic mode with CO_2. Considering the relatively large cell area (33 cm^2) in tubular geometry and fact that no reference electrode was used, a deconvolution of the EIS curve would be challenging and hence was not attempted.

At each test temperature, the tube cell was operated at 1.5 V in a dry CO_2 environment for 20 min, and the amount of CO produced was measured online using gas chromatography (GC). As expected, CO_2 to CO conversion gradually increased with temperature, attaining a maximum value of 70% at 800 °C (Fig. S2 in the ESI†) with a corresponding faradaic efficiency of 97%. Such a high conversion can be attributed to reduced polarisation and activation losses that created a more reducing environment for CO_2, and possibly also due to greater adsorption of CO_2 on GDC at higher temperatures. GDC is a redox-stable, mixed ionic electronic conductor (MIEC). It is believed[18,20–22] that in a reducing environment, Ce^{4+} is reduced to Ce^{3+}, leading to the formation of oxygen vacancies in the GDC lattice. These vacancies are then occupied by oxygen from CO_2 dissociation.

Based on the above results, Ag–GDC appeared to be a promising candidate for effective CO_2 electrolysis: the first crucial step for *in situ* methanation. Note that Ag has been previously reported to be catalytically inactive towards high-temperature CO_2 electroreduction;[7,11,23] the Ag in our composite electrode is no exception. To confirm our conjecture, CO_2 electrolysis was performed with bare Ag electrodes instead of the Ag–GDC composite in the same temperature range of 500–700 °C. The *V–I* curves are provided in Fig. 1B, and the EIS spectra at open-circuit voltage (OCV) are shown in Fig. S3 of the ESI.† Fig. 1B shows that although the *V–I* curves were similar in nature to those of the composite electrode, the current was almost an order of magnitude lower; the corresponding CO production rates at 1.5 V were also ~10 times less than when using Ag–GDC. Such poor performance of the Ag electrode can be attributed to the catalytic inertness of Ag as well as a stipulated reduction in the TPB. Being a pure electronic conductor, Ag alone cannot build up the electron–ion–gas TPB, which is a key to electrochemical reactions. In contrast, Ag–GDC is a mixed ionic electronic conductor that significantly increases the TPBs, thereby enhancing the electrochemical performance of the cell.

The experimental data obtained with Ag electrodes corroborate the idea that Ag did not contribute to the enhanced CO_2 electroreduction envisaged when using the Ag–GDC composite electrodes and that the cardinal role was played by the versatile material GDC. Based on these initial results, we concluded that the Ag–GDC composite electrode was worthy of investigation for *in situ* methanation.

2.2 Performance of the Ag–GDC composite electrode for methanation

An identical tube cell was tested at 500, 600 and 700 °C with a H_2/CO_2 (4 : 1) mixture. Fig. 2A–C present the open-circuit EIS spectra at 500, 600 and 700 °C, respectively. Fig. 2D and E demonstrate the corresponding *V–I* and *V–I* curves corrected for wire resistance.

The magnitude of both HF (~1000 to 5 Hz) and LF (~5 to 0.1 Hz) arcs of the impedance spectra decreased with a rise in temperature (Fig. 2A–C). As predicted from the curve fitting of the EIS spectra, the R_{pol} at OCV was 17.72, 6.50 and 1.02 Ω cm^2 at 500, 600 and 700 °C respectively. At all temperatures, the bulk of R_{pol} came from the LF arc, as noted by Yue *et al.*[19] With an

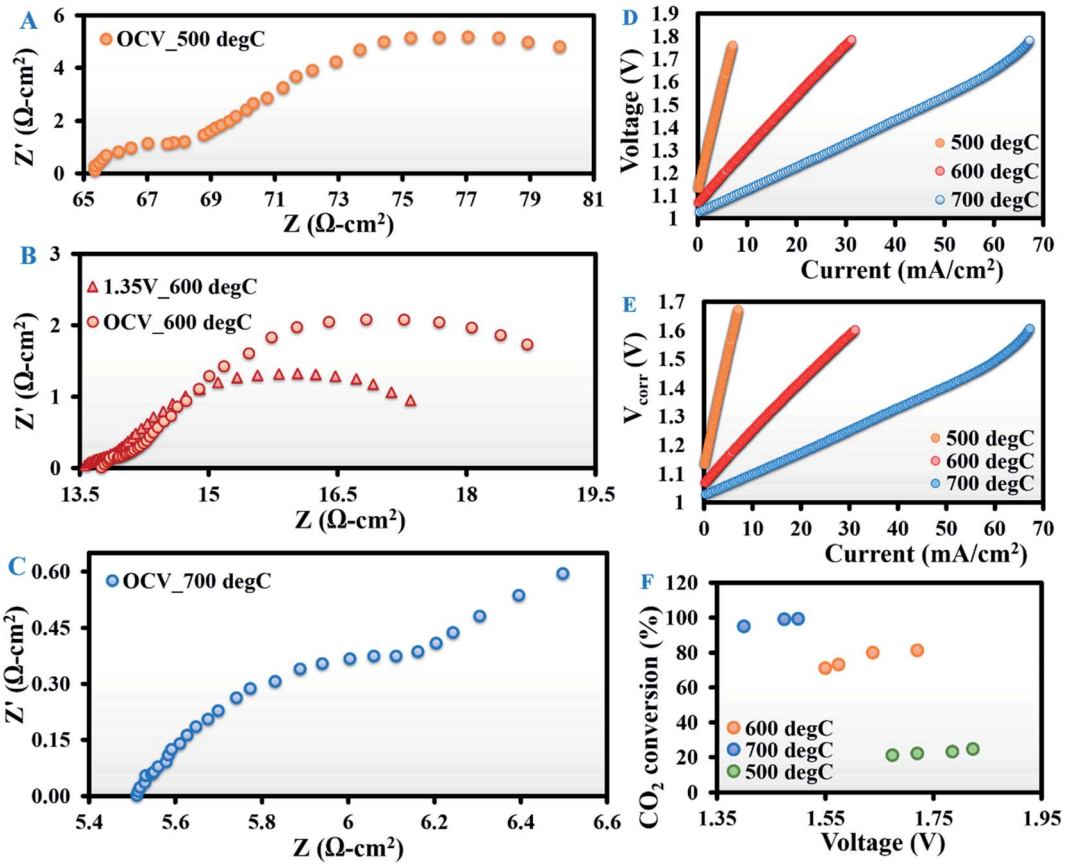

Fig. 2 Electrochemical impedance spectra at open-circuit voltage of a tubular solid oxide electrolysis cell with the Ag–GDC composite electrode recorded during electrochemical reduction of H_2/CO_2 in a ratio of 4 : 1 at (A) 500, (B) 600 and (C) 700 °C, with the corresponding (D) actual and (E) current–voltage characteristics (wire-resistance corrected). (F) CO_2 conversion as a function of applied voltage at 500, 600 and 700 °C.

increase in applied potential from OCV to 1.35 V at 600 °C, R_{pol} decreased from 6.5 to 4 Ω cm^2 due to a major reduction in the LF arc (Fig. 2B). This can be attributed to improved cell kinetics at higher potentials.

Another interesting observation from the EIS spectra was a substantial drop in the open-circuit R_{pol} from dry CO_2 to H_2/CO_2 atmospheres (Table 1). At OCV, when dry CO_2 is fed to the cathode, only CO_2 electroreduction (eqn (3)) occurs, whereas, when a H_2/CO_2 mixture with H_2 concentration as high as 80% is introduced at the cathode, the dominant reaction is the oxidation of H_2 by the oxide ions (eqn (6)) generated from CO_2 electroreduction. The latter is kinetically more active than the former, resulting in lower R_{pol}.

$$H_2 + O^{2-} = H_2O + 2e^- \quad (6)$$

Table 1 Ohmic (R_{ohm}) and polarisation (R_{pol}) resistances under CO_2 and H_2/CO_2 atmospheres under open-circuit voltage conditions between 500 and 700 °C

Gas composition	Temperature (°C)	R_{ohm} (Ω cm^2)	R_{pol} (Ω cm^2)
CO_2	500	68.15	63.79
H_2/CO_2 (4 : 1)	500	68.15	17.72
CO_2	600	13.74	50.95
H_2/CO_2 (4 : 1)	600	13.74	6.50
CO_2	700	5.63	11.12
H_2/CO_2 (4 : 1)	700	5.515	1.02

Another possibility is that the presence of a reducing gas such as H_2 increases the rate of Ce^{4+} to Ce^{3+} reduction, which makes CO_2 surface adsorption thermodynamically more favourable and faster, as noted in recent density functional theory studies.[24] This helps to reduce the overall cell polarisation resistance. However, we surmise that the lower surface diffusion resistance of smaller H_2 molecules compared with CO_2 molecules might also contribute to the drop in R_{pol}. Previously, Matsuzaki *et al.*[25] observed higher impedance with CO than with H_2 while studying the electrochemical oxidation of these two gases in fuel cell mode (solid oxide fuel cell). They concluded that CO encounters higher diffusion resistance than H_2 while moving across the electrode surface.

GC analysis of the outlet gases evolving at the cathode revealed that at OCV, CO_2 conversions were 20, 51 and 66% at 500, 600 and 700 °C, respectively, with the corresponding CO production rates of 3.2, 7.9 and 9.8 ml min^{-1}. At OCV, zero

electroreduction of CO_2 is plausible; therefore, the source of this CO must be the RWGS reaction (eqn (2)). However, with an increase in applied potential, more CO_2 was converted (Fig. 2F) due to enhanced electroreduction. At 500 °C, the increase was minimal (from 21% at 1.67 V to 24.5% at 1.82 V). However, at 600 °C, CO_2 conversion increased significantly from 71% at an applied potential of 1.55 V to 81% at 1.72 V. At 700 °C, the effect once again decreased, possibly due to the complete consumption of CO_2 by H_2 itself for the RWGS reaction. This is also clear from the fact that at 700 °C, CO_2 conversion reached ~99% at an applied potential of 1.48 V. This observation is in line with literature reports[26–30] for H_2/CO_2 electrolysis conducted with different electrode materials, but has been shown here for the first time with an Ag–GDC composite.

Based on GC analysis, under all test conditions, the faradaic efficiency was ~99% and carbon balance fairly matched 100% within the limits of experimental accuracy, signifying trivial or no carbon deposition. This is consistent with previous reports confirming the anti-coking properties of ceria.[16,21,22,31–33]

One of the key findings of this research is the *in situ* generation of methane between 500 and 700 °C under an H_2/CO_2 (4 : 1) environment (Table 2) in the absence of any specific methanation catalyst, such as Ni or Fe. Also, according to the literature, Ag has absolutely no catalytic activity towards either CO_2 or CO methanation although it catalyses CO_2 and CO hydrogenation to methanol to a limited extent.[34–36] The most commonly studied catalysts for methanation carried out in a thermochemical reactor at 1 bar and at 200–500 °C are Ni or its bimetallic substitutes (Ni/Ru or Ni/Co or Ni/Mn), on oxide supports such as alumina, silica, titania or zirconia.[37–41]

At all test temperatures, no methane was detected at OCV. This clearly establishes that methane evolution is a purely electrochemical phenomenon under the influence of applied potential. The maximum methane generation of 1.08×10^{-7} millimole s^{-1} cm^{-2} was recorded at 700 °C under an applied potential of 1.9 V with respect to OCV. Such low methane production can be attributed to the synergistic effect of the thickness (0.9 cm) of the electrolyte and the insufficient catalytic activity of the electrode towards H_2 dissociation and H^+ ion spillover,[42–45] which play pivotal roles in methanation. Thinning down the electrolyte would increase the current density, and thereby the methane yield. However, our intention here was not to maximise the methane yield, but to investigate whether Ag–GDC is electrocatalytically conducive to *in situ* methanation and determine how such *in situ* methane synthesis is governed purely electrochemically.

The first trace of methane was attained at different applied currents and correspondingly different voltages for the three different test temperatures, as shown in Table 2 in blue font. This indicates that the current at which methane starts evolving is a function of the operating temperature and hence of thermodynamic equilibrium. The sources of *in situ* generated methane include CO_2 hydrogenation (eqn (1)) and CO hydrogenation (eqn (4)), both of which are exothermic reactions and thus less favourable at higher temperatures. On the other hand, the methane can dissociate by two possible endothermic reactions: cracking (eqn (8)) or steam reforming (eqn (7)). Steam is also generated *in situ* as a methanation by-product. Thus, it is highly likely that methane is being produced even at currents lower than where it is initially detected, but it undergoes thermodynamic equilibrium-dictated dissociation until the current is sufficiently high to electrolyse and remove steam from the system. Since the tube was almost 30 cm long, the residence time of nascent methane was sufficient to increase the probability of such dissociation. What further corroborated this idea was the observation that with an increase in temperature, the minimum current (I_{min}) at which methane started evolving gradually increased, which was consistent with the gradual increase in the equilibrium constants (K_{eql})[46] of the methane-dissociation reactions (eqn (7) and (8)) as shown in Table 3.

$$CH_4 + 2H_2O = CO_2 + 4H_2 \ (\Delta H_{1023K} = 164 \text{ kJ mol}^{-1}) \quad (7)$$

$$CH_4 = 2H_2 + C \ (\Delta H_{1023K} = 74.8 \text{ kJ mol}^{-1}) \quad (8)$$

However, beyond I_{min}, the increase in methane production did not exhibit a linear relationship with current density. For complex materials such as Ag–GDC endowed with mixed ionic and electronic (MIEC) properties, a higher applied potential both increases the current density and remarkably improves the electrocatalytic activity towards CO_2 electrolysis, as explained in Section 2.1. This results in higher production of CO, which further increases methane generation. Thus, at current

Table 2 Volumetric percentages of CO and CH_4 as obtained by gas chromatography for H_2/CO_2 electrolysis under varying conditions of voltage between 500 and 700 °C using Ag–GDC composite electrodes (OCV = open-circuit voltage)

Temp (°C)	Voltage (V)	Current (mA cm^{-2})	CO (%)	CH_4 (%)	CO (millimole s^{-1} cm^{-2})	CH_4 (millimole s^{-1} cm^{-2})	S_{CH4} (%)	Y_{CH4} (%)
500	1.10 (OCV)	0.00	5.80	0.000	6.54×10^{-5}	0	0	0
	1.79	6.06	6.36	0.016	7.17×10^{-5}	1.80×10^{-7}	0.25	0.06
	1.82	6.45	6.61	0.020	7.45×10^{-5}	2.25×10^{-7}	0.29	0.07
600	1.06 (OCV)	0.00	12.40	0.000	1.40×10^{-4}	0	0	0
	1.58	19.03	15.4	0.010	1.74×10^{-4}	1.13×10^{-7}	0.09	0.07
	1.72	25.36	16.80	0.030	1.89×10^{-4}	3.38×10^{-7}	0.15	0.13
700	1.02 (OCV)	0.00	14.80	0.000	1.67×10^{-4}	0	0	0
	1.50	40.91	19.90	0.020	2.24×10^{-4}	2.25×10^{-7}	0.09	0.08
	1.90	60.61	19.80	0.096	2.23×10^{-4}	1.08×10^{-6}	0.50	0.49

Table 3 Equilibrium constants (K_{eql}) and thermodynamic conversions of methanation and methane-dissociation reactions between 500 and 700 °C

	500 °C		600 °C		700 °C	
Reaction	K_{eql}	Conversion (%)	K_{eql}	Conversion (%)	K_{eql}	Conversion (%)
CO_2 methanation	62.40	83.0	3.35	71.9	0.33	60.0
CO methanation	376.00	90.5	9.56	78.0	0.52	60.0
CH_4 steam reforming	0.02	7.3	0.30	12.5	3.04	19.0
CH_4 cracking	0.15	17.4	0.60	30.8	1.58	46.1

densities greater than I_{min}, the increase in the methane production rate was not directly proportional to the increment in current density; rather, it was higher than that.

Based on all our aforementioned observations, it can be rightly concluded that the *in situ* methane synthesis observed here is a completely electrochemical phenomenon, governed by the overall thermodynamic equilibrium of the methanation and methane-dissociation reactions taking place while the cell is in operation. The minimum current (I_{min}) at which methane begins evolving, as well as the overall methane generation, is also dictated by thermodynamic equilibrium. Similar observations have never been previously reported with an Ag–GDC composite electrode or any other electrode. X-ray diffraction (XRD) and scanning electron microscopy (SEM) results are discussed in the ESI (Fig. S5†), since they revealed no significant morphological or phase changes between fresh and used electrodes.

2.3 Possible impact of oxygen stripping on the thermodynamic equilibrium governing electrochemical methane synthesis

The mixed ionic electronic conductivity of GDC makes the Ag–GDC composite a complex material. To investigate how the thermodynamic equilibrium could be shifted to increase methane generation, we deemed it necessary to eliminate any catalytic and/or electrocatalytic effects induced by GDC on CO_2 electrolysis by virtue of its redox ability because such effects might impact the methane generation rate under varying conditions of temperature and applied potential. For this evaluation, H_2/CO_2 (4 : 1 v/v) electrolysis was carried out with bare Ag electrodes on the YSZ electrolyte in the same temperature range of 500 to 700 °C. We aimed to determine whether methane generation was affected by the rate of oxide ion removal from the cell.

The EIS curves recorded at OCV are provided in Fig. S4 of the ESI.† The *V–I* data (Fig. 3A) show that for all three test temperatures, the current at any particular voltage was almost an order of magnitude lower when using bare Ag than the corresponding values obtained with the Ag–GDC composite. This resulted in scanty CO_2 electroreduction with no methanation observed at 500 °C. The first trace of methane was obtained at an applied potential of 2.3 V (1.69×10^{-7} millimole s^{-1} cm^{-2}) and 1.85 V (2.25×10^{-7} millimole s^{-1} cm^{-2}) at 600 and 700 °C, respectively. The corresponding currents (I_{min}) recorded were 7.88 and 9.7 mA cm^{-2}, respectively.

Interestingly, at 700 °C, when the current was increased beyond 9.7 mA cm^{-2} (I_{min}), methane generation increased proportionally (Fig. 3B). This indicates that above I_{min}, methane generation increases in proportion with the increment in O^{2-} removal, since in solid oxide ion conducting electrolytes, oxygen removal varies proportionally with current, as determined from Faraday's law.[47]

This is a novel observation that has never been reported in the literature. Similar observations at 600 °C would require cell operation at potentials above 2.3 V, which might cause rapid removal of O^{2-} ions from the electrolyte (YSZ) itself, leading to zirconia blackening.[48,49] A plausible alternative is the use of a thin YSZ electrolyte that guarantees less ohmic resistance and thus higher current densities at lower voltages.

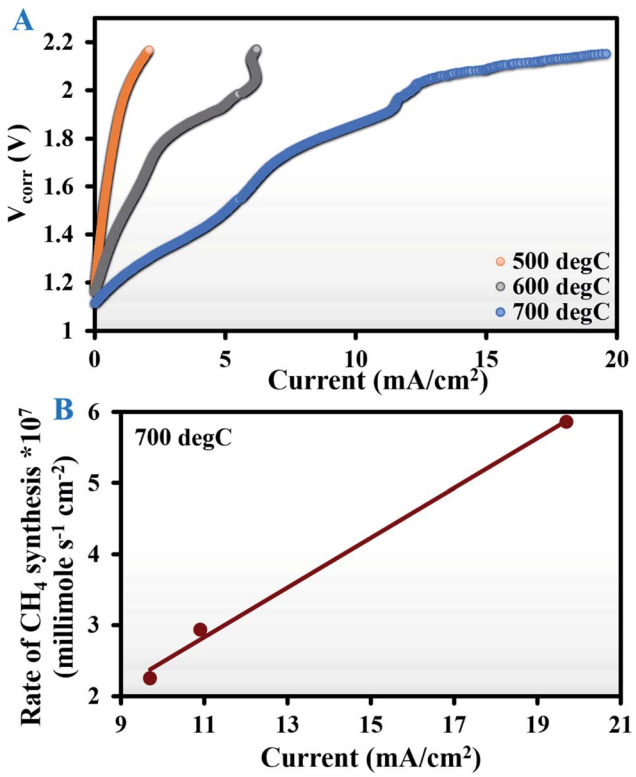

Fig. 3 (A) Voltage–current curves (corrected for lead wire resistance) for a tubular solid oxide electrolysis cell with the Ag electrode recorded during electrochemical reduction of a H_2/CO_2 mixture (4 : 1 v/v) at 500, 600, and 700 °C. (B) The rate of methane synthesis (millimole s^{-1} cm^{-2}) at 700 °C shows a linear trend as a function of current beyond an applied potential of 1.85 V.

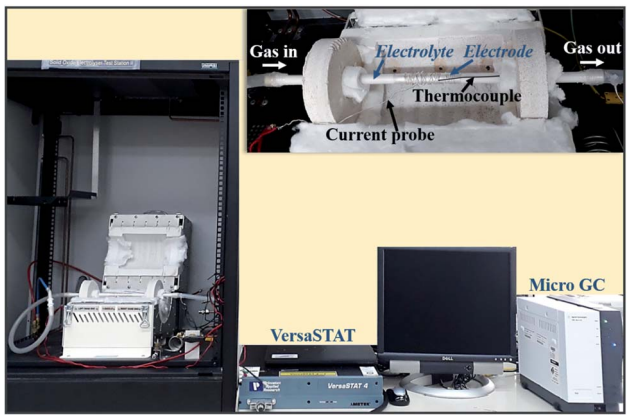

Fig. 4 Tube cell test set-up comprising a furnace, VersaSTAT and Micro-GC. The inset at the top right corner shows a magnified view of the tube cell positioned inside the furnace.

It was clear from our results that the extent of methane synthesis was directly related to the rate of oxygen removal from the system. However, for further verification, we carried out H_2/CO_2 (4 : 1) hydrogenation in a thermochemical methanation reactor in the absence of oxygen stripping at 1 bar and two different temperatures of 450 and 500 °C. A packed bed of glass wool and Ag–GDC powder (0.2 g) was housed inside the reactor (detailed set-up is described in the experimental section). The Ag–GDC powder had the same composition as the Ag–GDC electrodes used in our symmetric cells discussed in Sections 2.1 and 2.2. The H_2/CO_2 gas mixture was purged at a constant flow rate of 50 ml min^{-1} through the reactor. As detected through the online GC connected to the reactor outlet, the amounts of CO obtained at 450 and 500 °C were ~3 and 4.5%, respectively. The value at 500 °C was similar to that observed with Ag–GDC composite electrodes (5.8%) at the same temperature under OCV conditions. Interestingly, at both 450 and 500 °C, the methane produced was only around 0.001%, which was almost an order of magnitude less than the minimum amount of methane (0.016%) obtained at 500 °C using Ag–GDC composite electrodes (Table 2).

All the above observations hint towards the fact that if oxygen from the *in situ* generated steam (a by-product of methanation reactions) can be removed very quickly by rapid O^{2-} stripping across the electrolyte, then the forward methanation reactions (eqn (1) and (4)) will possibly be favoured according to Le Chatelier's principle,[50] and the dissociation of *in situ* evolved methane (eqn (6) and (7)) will be inhibited. Such a shift of thermodynamic equilibrium will be manifested by a directly proportional increase in methane production upon increasing current under the same applied potential.

3. Conclusion

We have tested for the first time an Ag–GDC composite electrode as a potential candidate for *in situ* methane synthesis in SOECs. This electrode composition was electrocatalytically very active at 500–700 °C towards both CO_2 electroreduction (during dry CO_2 electrolysis) and the RWGS reaction (H_2/CO_2 (4 : 1 v/v) electrolysis under no-load conditions, i.e., at OCV), which are the first crucial steps for effective *in situ* methane generation. GDC, by virtue of its mixed ionic electronic conductivity and high reducibility, imparts a high electrocatalytic activity to the Ag–GDC composite, whereas Ag only improves the electrode's adhesion properties and electronic conductivity.

When H_2/CO_2 (4 : 1 v/v) electrolysis was carried out with Ag–GDC electrodes at 500, 600 and 700 °C, some methane was obtained, but only under load conditions. The generation of methane in the absence of any methanation catalyst, such as Ni/Fe/Ru, leads us to conclude that the *in situ* methane synthesis envisaged in this work is a purely electrochemical phenomenon. The maximum methane production rate was 1.08×10^{-7} millimole s^{-1} cm^{-2} at 700 °C under an applied potential of 1.9 V. Interestingly, at any temperature, the first trace of methane was detected at a minimum value of current density (I_{min}), which increased monotonically with a rise in temperature. Based on this, we propose that H_2/CO_2 electrolysis is a dynamic process during which both methanation (exothermic) and methane-dissociation (endothermic) reactions take place simultaneously. However, the thermodynamically opposite nature of these reactions gradually makes methane evolution less favourable at higher temperatures. Thus, nascent methane produced in the SOEC environment undergoes thermodynamic equilibrium-dictated dissociation until the current is sufficiently high to electrolyse steam. The steam is a by-product of the methanation reaction and leads to methane dissociation *via* its reforming. Steam electrolysis essentially implies the removal of oxygen from the cell. Therefore, we can conclude that the extent of methane generation can be effectively shifted by increasing the rate of oxide ion removal through the electrolyte. Further strengthening this hypothesis is the observation that when H_2/CO_2 (4 : 1 v/v) electrolysis was carried out using bare Ag electrodes, methane generation beyond I_{min} increased in direct proportion with current density, or in other words, with the rate of oxygen removal from the cell. This is a completely new concept that is worthy of future investigation.

4. Materials and methods

4.1 Cell fabrication

Electrolyte-supported, open-ended tube cells were fabricated through isostatic pressing of 8 mol% yttria-stabilised zirconia (8-YSZ) powder procured from Tosoh Corporation Japan at 170 MPa using an in-house designed die followed by sintering in air at 1500 °C for 2 h. The final dimensions of the tube cell were OD 11 mm, length 340 mm and electrolyte thickness 0.45 mm. The electrode ink was prepared by mixing Ag powder (Alfa Aesar) and gadolinia-doped ceria ($Gd_{0.1}Ce_{0.9}O_{2-\delta}$) purchased from Fuel Cell Materials Inc. (FCM) in a weight ratio of 3 : 7 along with a terpinol-based ink vehicle (FCM), followed by ball milling the mixture for 2 h.[51] The as-prepared ink was brush-painted on the inside and outside active areas of the sintered electrolyte tubes over a length of 12 cm and sintered at 825 °C for 2 h at heating and cooling rates of 180 °C min^{-1}. The final

thickness of each electrode was between 30 and 50 μm, with an equivalent active area of 33 cm^2. The current was collected through silver wires that were spirally wound on both sides of the tube spanning the electrode area. Silver paste was then used to improve further adhesion and contact of the current collector with the electrode.

4.2 Physical and electrochemical characterisation

Powder XRD of the Ag–GDC composite cathode after cell testing was performed using a benchtop XRD (Bruker D2 Phaser) with a Cu-Kα radiation source. The diffractogram was recorded between 10 and 80° at a scan rate of 2° min^{-1}. The microstructure of the electrode was imaged using a ZEISS SEM. All electrochemical measurements, such as *V–I* curves, chronoamperometry and impedance spectroscopy (EIS curves), were conducted using a Princeton Applied Research VERSAStat. *V–I* measurements were recorded at 5 mV s^{-1}, and impedance measurements were carried out in the frequency range of 1000–0.1 Hz at an amplitude of 70 mV.

4.3 Cell performance testing

All electrochemical measurements were carried out using symmetric tube cells fabricated in-house. In the present set-up (Fig. 4), the test gases (dry CO_2 or an 80% H_2/20% CO_2 mixture) were purged into the fuel electrode (cathode), while the air electrode (anode) was exposed to the atmosphere. The first set of measurements were performed at four different temperatures of 500, 600, 700 and 800 °C by purging dry CO_2 (industrial grade, BOC) at a constant flow rate of 50 ml min^{-1} using Ag–GDC composite electrodes and an 8-YSZ electrolyte. Next, the same experiments were repeated under identical conditions of temperature and flow rate, but with bare Ag electrodes. In the next phase, electrochemical measurements for methanation tests were performed using the Ag–GDC composite electrode and 8-YSZ electrolyte at 500–700 °C by purging an 80% H_2/20% CO_2 mixture (industrial grade, BOC) at a constant flow rate of 50 ml min^{-1}. The same experiments were repeated for bare Ag electrodes.

The mass-flow meters used were calibrated using separate, certified flow meters. The temperature at the centre of the cathode was monitored using a single K-type thermocouple and is designated henceforth as the operating temperature. At each temperature, after recording the *V–I* curves and EIS spectra at OCV, the cell was loaded at different voltages for 30 min and the composition of the gases evolving at the cathode was analysed using a GC (Agilent Micro-GC). The impedance plots were recorded under no-load conditions (OCV). All *V–I* curves were recorded against OCV obtained under the particular cell testing conditions of temperature and gas mixture.

4.4 Ag–GDC testing in a thermochemical methanation reactor

Ag powder (Alfa Aesar) and GDC ($Gd_{0.1}Ce_{0.9}O_{2-\delta}$) purchased from FCM were mixed in a weight ratio of 3 : 7 followed by ball milling for 2 h. The mixture was then sintered at 825 °C for 2 h at heating and cooling rates of 180 °C min^{-1}. The as-prepared Ag–GDC composite powder was subsequently tested for the CO_2 hydrogenation reaction using a fixed-bed, custom-designed, stainless-steel reactor lined internally with brass sleeves. The powder (0.2 g) was evenly dispersed into a bed of glass wool plugged inside the reactor. The reaction temperature was measured with a K-type thermocouple buried into the glass wool bed. The reactor was held within a furnace equipped with a temperature controller. The flow rates were controlled using Bronkhorst High-Tech Series mass-flow controllers. The Ag–GDC bed was heated at 300 °C (ramp rate ~ 3 °C min^{-1}) and 1 bar pressure for 2 h under a 100 ml min^{-1} Ar (Air Liquide 99.9% purity) flow. Following this, the temperature was further increased to the desired set point while keeping the argon flow rate constant. Subsequently, the gas flow was changed to 50 ml min^{-1} of H_2/CO_2 (4 : 1 v/v, purchased from BOC) and 50 ml min^{-1} of Ar. CO_2 hydrogenation was conducted and the performance of the catalysts was tested under steady-state conditions. The reaction products were analysed online using gas chromatography using an Agilent 7890A GC-TCD/FID fitted with HayeSep N, MolSieve 5A and Porapak Q columns. Nitrogen was used as an internal standard for chromatographic analyses. The gas was sampled online at intervals of ~35 min for a period of 2 h. Subsequently, the reactor was cooled under a 100 ml min^{-1} Ar flow.

Funding

This work received funding from the Australian Renewable Energy Agency (ARENA) as part of ARENA's Research and Development Program—Renewable Hydrogen for Export, and also from the CSIRO Hydrogen Energy Systems Future Science Platform, CSIRO Research Office, and a PhD scholarship from Monash University. The funder was not involved in the study design, collection, analysis, and interpretation of data, the writing of the manuscript, or the decision to submit it for publication.

Conflicts of interest

There are no conflicts to declare.

Acknowledgements

This Activity received funding from ARENA as part of ARENA's Research and Development Program – Renewable Hydrogen for Export, and also from CSIRO Hydrogen Energy Systems Future Science Platform. The authors would like to thank Daniel Roberts and Shambhu Singh Rathore for an internal review of the paper.

References

1 S. Biswas, A. Kulkarni, S. Giddey and S. Bhattacharya, A Review on Synthesis of Methane as a Pathway for Renewable Energy Storage with a Focus on Solid Oxide Electrolytic Cell-Based Processes, *Frontiers in Energy Research*, 2020, **8**, 570112.

2 K. Xie, Y. Zhang, G. Meng and J. T. Irvine, Direct synthesis of methane from CO_2/H_2O in an oxygen-ion conducting solid oxide electrolyser, *Energy Environ. Sci.*, 2011, **4**(6), 2218–2222.
3 D. M. Bierschenk, J. R. Wilson and S. A. Barnett, High efficiency electrical energy storage using a methane–oxygen solid oxide cell, *Energy Environ. Sci.*, 2011, **4**(3), 944–951.
4 W. Li, H. Wang, Y. Shi and N. Cai, Performance and methane production characteristics of H_2O–CO_2 co-electrolysis in solid oxide electrolysis cells, *Int. J. Hydrogen Energy*, 2013, **38**(25), 11104–11109.
5 L. Chen, F. Chen and C. Xia, Direct synthesis of methane from CO_2–H_2O co-electrolysis in tubular solid oxide electrolysis cells, *Energy Environ. Sci.*, 2014, **7**(12), 4018–4022.
6 B. Chen, H. Xu and M. Ni, Modelling of SOEC-FT reactor: pressure effects on methanation process, *Appl. Energy*, 2017, **185**, 814–824.
7 Y. Xie, J. Xiao, D. Liu, J. Liu and C. Yang, Electrolysis of carbon dioxide in a solid oxide electrolyzer with silver-gadolinium-doped ceria cathode, *J. Electrochem. Soc.*, 2015, **162**(4), F397–F402.
8 R. D. Green, C.-C. Liu and S. B. Adler, Carbon dioxide reduction on gadolinia-doped ceria cathodes, *Solid State Ionics*, 2008, **179**(17–18), 647–660.
9 C. de Leitenburg, A. Trovarelli and J. Kašpar, A temperature-programmed and transient kinetic study of CO_2 activation and methanation over CeO_2 supported noble metals, *J. Catal.*, 1997, **166**(1), 98–107.
10 P. U. Aldana, F. Ocampo, K. Kobl, B. Louis, F. Thibault-Starzyk, M. Daturi, *et al.*, Catalytic CO_2 valorization into CH_4 on Ni-based ceria-zirconia. Reaction mechanism by operando IR spectroscopy, *Catal. Today*, 2013, **215**, 201–207.
11 J. Zhang, Y. Ji, H. Gao, T. He and J. Liu, Composite cathode $La_{0.6}Sr_{0.4}Co_{0.2}Fe_{0.8}O_3$–$Sm_{0.1}Ce_{0.9}O_{1.95}$–Ag for intermediate-temperature solid oxide fuel cells, *J. Alloys Compd.*, 2005, **395**(1–2), 322–325.
12 Y. Luo, Y. Shi, Y. Chen, W. Li, L. Jiang and N. Cai, Pressurized tubular solid oxide H_2O/CO_2 coelectrolysis cell for direct power-to-methane, *AIChE J.*, 2020, **66**(5), e16896.
13 X. Yue and J. T. Irvine, Impedance studies on LSCM/GDC cathode for high temperature CO_2 electrolysis, *Electrochem. Solid-State Lett.*, 2012, **15**(3), B31.
14 Y. Song, X. Zhang, K. Xie, G. Wang and X. Bao, High-Temperature CO_2 Electrolysis in Solid Oxide Electrolysis Cells: Developments, Challenges, and Prospects, *Adv. Mater.*, 2019, **31**(50), 1902033.
15 L. Spiridigliozzi, E. Di Bartolomeo, G. Dell'Agli and F. Zurlo, GDC-Based Infiltrated Electrodes for Solid Oxide Electrolyzer Cells (SOECs), *Appl. Sci.*, 2020, **10**(11), 3882.
16 G. Kaur, A. P. Kulkarni, S. Giddey and S. P. S. Badwal, Ceramic composite cathodes for CO_2 conversion to CO in solid oxide electrolysis cells, *Appl. Energy*, 2018, **221**, 131–138.
17 L. Chen, F. Chen and C. Xia, Direct synthesis of methane from CO_2–H_2O co-electrolysis in tubular solid oxide electrolysis cells, *Energy Environ. Sci.*, 2014, **7**(12), 4018–4022.
18 A. Kulkarni, S. Giddey and S. P. S. Badwal, Efficient conversion of CO_2 in solid oxide electrolytic cells with Pd doped perovskite cathode on ceria nanofilm interlayer, *J. CO_2 Util.*, 2017, **17**, 180–187.
19 X. Yue and J. T. S. Irvine, Alternative cathode material for CO_2 reduction by high temperature solid oxide electrolysis cells, *J. Electrochem. Soc.*, 2012, **159**(8), F442.
20 O. A. Marina, C. Bagger, S. Primdahl and M. Mogensen, A solid oxide fuel cell with a gadolinia-doped ceria anode: preparation and performance, *Solid State Ionics*, 1999, **123**(1–4), 199–208.
21 C. Neofytidis, V. Dracopoulos, S. Neophytides and D. K. Niakolas, Electrocatalytic performance and carbon tolerance of ternary Au-Mo-Ni/GDC SOFC anodes under CH_4-rich internal steam reforming conditions, *Catal. Today*, 2018, **310**, 157–165.
22 J. B. Goodenough and Y.-H. Huang, Alternative anode materials for solid oxide fuel cells, *J. Power Sources*, 2007, **173**(1), 1–10.
23 F.-Y. Wang, S. Cheng and B.-Z. Wan, Porous Ag–CGO cermets as anode materials for ITSOFC using CO fuel, *Catal. Commun.*, 2008, **9**(7), 1595–1599.
24 N. Kumari, M. A. Haider, M. Agarwal, N. Sinha and S. Basu, Role of reduced CeO_2 (110) surface for CO_2 reduction to CO and methanol, *J. Phys. Chem. C*, 2016, **120**(30), 16626–16635.
25 Y. Matsuzaki and I. Yasuda, Electrochemical Oxidation of H_2 and CO in a H_2-H_2O-CO-CO_2 System at the Interface of a Ni-YSZ Cermet Electrode and YSZ Electrolyte, *J. Electrochem. Soc.*, 2000, **147**(5), 1630.
26 E. Ioannidou, S. Neophytides and D. K. Niakolas, Experimental clarification of the RWGS reaction effect in H_2O/CO_2 SOEC co-electrolysis conditions, *Catalysts*, 2019, **9**(2), 151.
27 T.-R. Lee, H.-N. Im, S.-Y. Jeon, Y.-S. Yoo, A. U. Chavan and S.-J. Song, Dependence of H_2O/CO_2 co-electrolysis performance of SOEC on microstructural and thermodynamic parameters, *J. Electrochem. Soc.*, 2016, **163**(7), F728–F736.
28 W. Zhang, Y. Zheng, B. Yu, J. Wang and J. Chen, Electrochemical characterization and mechanism analysis of high temperature co-electrolysis of CO_2 and H_2O in a solid oxide electrolysis cell, *Int. J. Hydrogen Energy*, 2017, **42**(50), 29911–29920.
29 Y. Wang, T. Liu, L. Lei and F. Chen, High temperature solid oxide H_2O/CO_2 co-electrolysis for syngas production, *Fuel Process. Technol.*, 2017, **161**, 248–258.
30 S. Hou and K. Xie, Enhancing the performance of high-temperature H_2O/CO_2 co-electrolysis process on the solid oxide $Sr_2Fe_{1.6}Mo_{0.5}O_{6-\delta}$-SDC/LSGM/$Sr_2Fe_{1.5}Mo_{0.5}O_{6-\delta}$-SDC cell, *Electrochim. Acta*, 2019, **301**, 63–68.
31 J. G. Lee, O. S. Jeon, H. J. Hwang, J. Jang, Y. Lee, S. H. Hyun, *et al.*, Durable and high-performance direct-methane fuel cells with coke-tolerant ceria-coated Ni catalysts at reduced temperatures, *Electrochim. Acta*, 2016, **191**, 677–686.
32 A. Elleuch and K. Halouani, Intermediate-temperature solid oxide fuel cell fueled by biofuels, in *Intermediate Temperature Solid Oxide Fuel Cells*, Elsevier, 2020. pp. 427–476.
33 M. Cimenti and J. M. Hill, Importance of pyrolysis and catalytic decomposition for the direct utilization of

methanol in solid oxide fuel cells, *J. Power Sources*, 2010, **195**(1), 54–61.

34 D. J. Goodman, *Methanation of carbon dioxide*, UCLA, 2013.

35 J. Wambach, A. Baiker and A. Wokaun, CO_2 hydrogenation over metal/zirconia catalysts, *Phys. Chem. Chem. Phys.*, 1999, **1**(22), 5071–5080.

36 K. Stangeland, D. Kalai, H. Li and Z. Yu, CO_2 methanation: the effect of catalysts and reaction conditions, *Energy Procedia*, 2017, **105**, 2022–2027.

37 A. Cárdenas-Arenas, A. Quindimil, A. Davó-Quiñonero, E. Bailón-García, D. Lozano-Castelló, U. De-La-Torre, *et al.*, Isotopic and in situ DRIFTS study of the CO_2 methanation mechanism using Ni/CeO_2 and Ni/Al_2O_3 catalysts, *Appl. Catal., B*, 2020, **265**, 118538.

38 W. L. Vrijburg, G. Garbarino, W. Chen, A. Parastaev, A. Longo, E. A. Pidko, *et al.*, Ni-Mn catalysts on silica-modified alumina for CO_2 methanation, *J. Catal.*, 2020, **382**, 358–371.

39 C. Lv, L. Xu, M. Chen, Y. Cui, X. Wen, C.-e. Wu, *et al.*, Constructing highly dispersed Ni based catalysts supported on fibrous silica nanosphere for low-temperature CO_2 methanation, *Fuel*, 2020, **278**, 118333.

40 L. Zeng, Y. Wang, Z. Li, Y. Song, J. Zhang, J. Wang, *et al.*, Highly Dispersed Ni Catalyst on Metal–Organic Framework-Derived Porous Hydrous Zirconia for CO_2 Methanation, *ACS Appl. Mater. Interfaces*, 2020, **12**(15), 17436–17442.

41 J. Ashok, S. Pati, P. Hongmanorom, Z. Tianxi, C. Junmei and S. Kawi, A review of recent catalyst advances in CO_2 methanation processes, *Catal. Today*, 2020, 471–489.

42 Y. Guo, S. Mei, K. Yuan, D.-J. Wang, H.-C. Liu, C.-H. Yan, *et al.*, Low-temperature CO_2 methanation over CeO_2-supported Ru single atoms, nanoclusters, and nanoparticles competitively tuned by strong metal–support interactions and H-spillover effect, *ACS Catal.*, 2018, **8**(7), 6203–6215.

43 X. Jia, X. Zhang, N. Rui, X. Hu and C.-j. Liu, Structural effect of Ni/ZrO_2 catalyst on CO_2 methanation with enhanced activity, *Appl. Catal., B*, 2019, **244**, 159–169.

44 H. Jiang, Q. Gao, S. Wang, Y. Chen and M. Zhang, The synergistic effect of Pd NPs and UiO-66 for enhanced activity of carbon dioxide methanation, *J. CO_2 Util.*, 2019, **31**, 167–172.

45 W. J. Lee, C. Li, H. Prajitno, J. Yoo, J. Patel, Y. Yang, *et al.*, Recent trend in thermal catalytic low temperature CO_2 methanation: a critical review, *Catal. Today*, 2020, DOI: 10.1016/j.cattod.2020.02.017.

46 J. Gao, Y. Wang, Y. Ping, D. Hu, G. Xu, F. Gu, *et al.*, A thermodynamic analysis of methanation reactions of carbon oxides for the production of synthetic natural gas, *RSC Adv.*, 2012, **2**(6), 2358–2368.

47 F. C. Walsh, The overall rates of electrode reactions: Faraday's laws of electrolysis, *Trans. IMF*, 1991, **69**(4), 155–157.

48 X. Vendrell and A. R. West, Induced p-type semiconductivity in yttria-stabilized zirconia, *J. Am. Ceram. Soc.*, 2019, **102**(10), 6100–6106.

49 J. Janek and C. Korte, Electrochemical blackening of yttria-stabilized zirconia–morphological instability of the moving reaction front, *Solid State Ionics*, 1999, **116**(3–4), 181–195.

50 J. De Heer, The principle of le chatelier and braun, *J. Chem. Educ.*, 1957, **34**(8), 375.

51 D. Fini, S. P. Badwal, S. Giddey, A. P. Kulkarni and S. Bhattacharya, Evaluation of Sc_2O_3–CeO_2–ZrO_2 electrolyte-based tubular fuel cells using activated charcoal and hydrogen fuels, *Electrochim. Acta*, 2018, **259**, 143–150.

